



Article

Implanting MnO₂ into Hexagonal Boron Nitride as Nanoadditives for Enhancing Tribological Performance

Xiaorong Chen ¹, Wenting Chen ¹, Linyi Zhang ¹, Minli Zeng ¹, Shiming Yang ¹, Zhanhe Yang ¹, Oluwafunmilola Ola ² , Kunyapat Thummavichai ³, Nannan Wang ^{1,*}  and Yanqiu Zhu ^{1,3,*}

- ¹ Guangxi Institute Fullerene Technology (GIFT), Key Laboratory of New Processing Technology for Nonferrous Metals and Materials, Ministry of Education, School of Resources Environment and Materials, Guangxi University, Nanning 530004, China; chenxiaorong0704@163.com (X.C.); chenwt@st.gxu.edu.cn (W.C.); zhanglinyi@st.gxu.edu.cn (L.Z.); minlizeng@st.gxu.edu.cn (M.Z.); 2015301085@st.gxu.edu.cn (S.Y.); 2039200206@st.gxu.edu.cn (Z.Y.)
- ² Advanced Materials Group, Faculty of Engineering, University of Nottingham, Nottingham NG7 2RD, UK; oluwafunmilola.ola1@nottingham.ac.uk
- ³ Department of Mathematics and Physical Sciences, College of Engineering, University of Exeter, Exeter EX4 4QF, UK; kt302@exeter.ac.uk
- * Correspondence: wangnannan@gxu.edu.cn (N.W.); y.zhu@exeter.ac.uk (Y.Z.)

Abstract: Hexagonal boron nitride nanosheets (h-BNNs) show great potential in the field of tribology due to their typical two-dimensional layered structure and are essential for replacing conventional sulfur/phosphate-containing additives. However, the large particle size and poor dispersion of h-BNNs seriously restrict their green lubrication application. In this paper, MnO₂@h-BNNs nanocomposites were successfully prepared by ultrasonically exfoliating a hydrothermal method. The tribological properties of MnO₂@h-BNNs nanocomposites as lubricant additives in poly- α -olefin oil (PAO) were investigated. The results show the oil dispersed with 0.25 wt% MnO₂@h-BNNs had the best friction reduction and antiwear effect with 42% and 11.2% reduction, respectively, compared with the plain oil. Through further wear surface analyzing, we verified the antiwear mechanism of additives in filling the micropits and grooves on the wear surface and forming a friction protection film including Fe₂O₃, MnO₂, and BN on the wear surface, avoiding direct contact between the friction subsets. This can provide ideas for other lubricating oil additives.

Keywords: hexagonal boron nitride (h-BN); manganese dioxide; lubricant additive; PAO6; tribological properties



Citation: Chen, X.; Chen, W.; Zhang, L.; Zeng, M.; Yang, S.; Yang, Z.; Ola, O.; Thummavichai, K.; Wang, N.; Zhu, Y. Implanting MnO₂ into Hexagonal Boron Nitride as Nanoadditives for Enhancing Tribological Performance. *Crystals* **2022**, *12*, 451. <https://doi.org/10.3390/cryst12040451>

Academic Editor: Xing-Wang Zhang

Received: 8 March 2022

Accepted: 22 March 2022

Published: 23 March 2022

Publisher's Note: MDPI stays neutral with regard to jurisdictional claims in published maps and institutional affiliations.



Copyright: © 2022 by the authors. Licensee MDPI, Basel, Switzerland. This article is an open access article distributed under the terms and conditions of the Creative Commons Attribution (CC BY) license (<https://creativecommons.org/licenses/by/4.0/>).

1. Introduction

Friction and wear are some of the main causes of energy loss and workpiece failure in mechanical systems, and the most effective way to control or reduce friction and wear is to use lubricants. The main role of lubricants is to reduce friction and wear on mutually moving surfaces, as well as to prevent corrosion, cool and remove system contamination [1–4]. In the modern industry, liquid lubricants are the most practical and effective type of lubricants for reducing friction and wear and extending the service life of equipment. However, traditional lubricants are no longer able to meet the demands of industrial development. Thus, the addition of additives to lubricants has become the main way to improve the quality and increase the variety of traditional lubricants. Additives are used in order to improve the performance of the base lubricant, such as oxidative stability, or antifriction and antiwear capabilities [5,6]. Traditional organic lubrication additives, such as zinc dialkyl dithiophosphate salts (ZDDP, ZnDTP, and MoDTC), contain zinc and a large amount of sulfur and phosphorus elements, which cause water pollution and lead to serious environmental problems [7,8]. In recent years, nanomaterials, due to their unique properties, such as small size, large specific surface area, and small van der Waals forces between the

layers and sheets, can effectively reduce the coefficient of friction and also improve the load-bearing capacity of the contact surface, which in turn can substantially improve the antiwear and friction reduction performance, especially that of layered nanomaterials, such as graphene [9–11], transition metal disulfide MS_2 ($M = Mo, W$) [12–14], hexagonal boron nitride (h-BN) [15,16], and black phosphorus [17,18]. Compared to conventional organic lubrication additives, 2D layered nanosheets are chemically more stable, which leads to less harmful emissions and reduced environmental pollution. This makes them to be better candidates in terms of environmental protection and sustainability.

h-BN has a structure similar to that of graphite and is a typical two-dimensional layered material with excellent thermal stability, good thermal conductivity, high oxidation resistance, high temperature resistance, and good mechanical strength [19,20]. As a lubricating additive, h-BN has weaker interlayer van der Waals forces than the covalent bonding between nitrogen and boron in the layer, which makes it easy to shear when subjected to load and can fill the wear surface better [21,22]. In addition, h-BN has been widely studied in the field as a green lubricant additive because it does not contain toxic microelements such as phosphorus and sulfur elements, and it is thermally stable and can maintain structural stability under high-temperature conditions. However, common h-BN is not conducive to lubrication due to its own large particle size. Manoj Kumar Gupta et al. [23] also studied and confirmed this problem. The size of h-BN affects the antiwear and friction reduction performance of lubricants. The smaller its particle size, the easier it is to transfer to the friction surface to form a friction protection film, thus improving the lubrication performance. To solve this application problem, Chao Linliu et al. [24] effectively improved the tribological properties of PAO10 base oil by ultrasonically exfoliating hexagonal boron nitride nanosheets (h-BNNs) as an additive. However, h-BNNs have high surface energy and can be easily agglomerated, making them difficult to disperse stably in the base oil for a long time. This hinders their further application in the industry.

In practice, in order to achieve the desired lubrication effect, different types of nanoparticles are usually prepared as nanomaterials containing two or more types of nanomaterials, which are collectively referred to as composite nanoadditives. Composite nanoadditives combine the properties of two or more nanoparticles, and the synergistic effect between the additives results in better friction reduction and antiwear properties than single nanoparticles. Ramachandra Arvind Singh's group [25] studied nanodiamond particles as secondary additives, added to PAO6 with CuO and h-BN, and found that nanodiamonds had a good synergistic relationship with the primary additives, effectively improving the lubrication effect. Nanoparticles such as metal monomers and their oxides have been shown to be effective lubricant additives [26]. By coating these nanoparticles on the surface of layered materials, i.e., h-BNNs, the aggregation of nanoparticles and nanosheets can be effectively inhibited [27–30]. The effective combination of nanosheets and nanoparticles not only retains their inherent and unique lubrication advantages, but also promises to produce synergistic effects [31,32]. Therefore, in tribological research, the synergistic effect of different nanoparticles in composite nanoadditives will become the focus of future research in this field.

In this paper, h-BNN composites doped with MnO_2 particles ($MnO_2@h-BNNs$) were successfully synthesized using ultrasonic exfoliation and hydrothermal synthesis to analyze their tribological behavior as poly-alpha olefin 6 (PAO6) oil nanoadditives at 100 °C. The lubrication mechanisms of h-BNNs and MnO_2 in this case were explored to determine their optimal content in PAO6 oil. In addition, the dispersion and stability of the composite $MnO_2@h-BNNs$ in PAO6 were analyzed using transmissivity and natural sedimentation methods. The frictional behavior of the lubricating oil system was also investigated by variable-temperature simulation tests.

2. Experiment

2.1. Experimental Materials

All reagents used in the experiments were analytical-grade and did not require further treatment. The reagents included: hexagonal boron nitride (h-BN) with particle size of 1~2 μm , isopropyl alcohol (IPA), potassium permanganate (KMnO_2), hydrochloric acid (HCl), petroleum ether (60–90 $^\circ\text{C}$), surface dispersant polyoxyethylene sorbitan fatty acid ester (Span80), and poly-alpha olefin 6 (PAO6) base oil (shear viscosity of 6.026 $\text{mPa}\cdot\text{s}$ at 100 $^\circ\text{C}$), which were provided by Nanning Yuchai Research Institute. The water used in the experiments was ultrapure water.

2.2. Preparation of Material

In this paper, MnO_2 @h-BNNs nanocomposites were prepared using ultrasound-assisted peeling method. The mechanism involves generating dense bubbles in the solvent through ultrasound, and the collapse of the bubbles generates a force to exfoliate the large lamellar material mixed in the solvent to create a two-dimensional material. The key to achieving efficient peeling is the matching of surface energy between the laminate and the solvent. The specific steps of this experiment using IPA-assisted stripping of hexagonal boron nitride are as follows: First, about 3 g of h-BN powder was added to a beaker containing 200 mL of IPA, and then 100 mL of deionized water was added and mechanically stirred well. Then, the mixture was ultrasonically dispersed by an ultrasonic disperser for 12 h at a power of 600 W for 20 s with an interval of 5 s. Centrifugation was used to collect supernatant from the mixed solution. The supernatant was centrifuged again to obtain the desired sample, which was washed with deionized water and then placed in vacuum for drying to obtain h-BNNs. The as-prepared 1.5 g of h-BNNs and KMnO_2 was added to 35 mL of deionized water and stirred for 10 min to obtain a mixed solution. During the stirring process, 0.5 mL of HCl was added drop by drop, and stirred for 10 min. Well-mixed solution was transferred to a 100 mL reaction kettle and maintained at 85 $^\circ\text{C}$ for 40 min. Finally, MnO_2 @h-BNNs nanocomposites were obtained by rinsing with deionized water three times and drying under vacuum at 40 $^\circ\text{C}$.

Lubricant sample preparation: PAO6 lubricant with good high- and low-temperature performance, viscosity–temperature performance, and nontoxic and nonirritating properties was used as base oil. This lubricant is the most commonly used synthetic lubricant for base oil with the widest range of use. In this experiment, oil samples containing Span80, h-BN powder, and MnO_2 @h-BNNs were prepared by controlling the addition of dispersant Span80 to compare their lubricating effects as additives. In addition, in this experiment, MnO_2 @h-BNNs additives with different contents (0.1 wt%, 0.25 wt%, and 0.5 wt%) were dispersed into PAO6 liquid oil using ultrasonic dispersion for 20 min and mechanical stirring for 10 min, and well-dispersed oil samples were obtained.

2.3. Tribological Performance Tests

In order to investigate the lubricating performance of MnO_2 @h-BNNs as a lubricant additive, the tribological properties were tested by using MR-10 four-ball friction tester and 280 W pointer-type antiwear tester. The steel balls were AI SI 52,100 steel with a 12.7 mm diameter and 62 HRC hardness. During the friction tester test, the bottom three balls were fixed in the oil box and completely submerged into the oil sample, and the fourth top ball was fixed onto the drive spindle, which rotated under the selected load and speed. The whole test process was monitored by a computer, and the friction coefficient (FC) was recorded automatically. We referred to the ASTM D4172 standard method, combined with the work of Manilal Murmu [33] and Li Wang et al. [21]. The friction experiments were performed at a test temperature of 100 $^\circ\text{C}$, a load of 392 N, a speed of 1200 rpm, and a time of 30 min.

The oil samples were tested using a 280 W pointer-type antiwear tester to study the wear of the friction contact surface and the change in oil temperature. The test conditions were room temperature, load of 980 N, and actual work for 5 min. Each of the above

experiments was repeated three times to ensure its accuracy. After the experiments, the diameter of the abrasion marks was measured with a metallographic microscope, and the friction parts were cleaned with petroleum ether and ethanol and then sealed for further testing.

2.4. Performance Characterization

The wear surface morphology of the samples and steel balls were analyzed by two types of field-emission scanning electron microscopes (SEM, SU8020 Hitachi, Osaki, Japan and FEI Quanta FEG 250, Tokyo, Japan). Raman spectrometer (inVia Reflex 1500080S, Nottingham, UK) was used to analyze the structure of the samples. X-ray photoelectron spectroscopy (XPS, ESCALAB 250XI ThermoFisher, Waltham, MA, USA) with Al as the radiation source was used to analyze the changes in the surface chemical valence of steel ball wear marks, and the obtained data were calibrated by C1s (284.8 eV). A laser confocal (KEYENCE VK-X1000) was used to analyze the wear marks on the steel balls, and a PerkinElmer Lambda UV-VIS spectrometer was used to determine the transmission spectra of the samples, and the transmission rate of PAO6 base oil was used as a substrate calibration to study the dispersion stability of the samples.

3. Results and Discussion

3.1. Characterization of MnO_2 @h-BNNs

Figure 1a shows the XRD patterns of h-BN powder, MnO_2 , and composite MnO_2 @h-BNNs, where the diffraction peaks of h-BN are consistent with the data of JCPDS card No. 09-0012. The diffraction peak of MnO_2 matches the data of JCPDS card number 42-1317 due to its low crystallinity, which may be birnessite-typed MnO_2 [34,35]. Moreover, the crystallographic surfaces of MnO_2 @h-BNNs and h-BN powder basically match, indicating that the prepared MnO_2 @h-BNNs are well-crystallized and still maintain the original hexagonal crystal shape. It is noteworthy that the diffraction peak of MnO_2 is difficult to observe in the figure, probably due to the weak intensity of its diffraction peak and the small amount of doping, which made it impossible to detect its signal. Compared with the XRD spectrum of h-BN, it is obvious that the (002) crystal plane of MnO_2 @h-BNNs is significantly enhanced compared to other diffraction peaks; comparing the value of $002/100$, that of MnO_2 @h-BNNs is 12.49, which is larger than that of h-BN at 10.29. This indicates that the h-BN was stripped along the (002) plane during the preparation process and the crystal plane increased and the h-BN lamellae decreased [36]. Figure 1b shows the Raman spectra of h-BN powder and composite MnO_2 @h-BNNs. The Raman peak of h-BN powder appears at 1365.42 cm^{-1} , which is mainly due to the E_{2g} vibrational mode of h-BN [37]. Compared with h-BN powder, MnO_2 @h-BNNs has a peak at 650.69 cm^{-1} , which is the Raman peak corresponding to MnO_2 [38].

To further demonstrate the composite MnO_2 @h-BNNs, the material was tested by XPS, as shown in Figure 1c–f, which shows the XPS-fitted curves of B, N, Mn 2p, and Mn 3s, respectively. As can be seen in Figure 1c, the two peaks splitting into B 1s at 190.5 eV and 190.95 eV are attributed to the B–N and B–O bonds, respectively. In the nitrogen region of the material, the peaks located at 398.0 eV and 398.5 eV are the B–N and NH–CO bonds, respectively (Figure 1d). In addition, the spectrum of Mn 3s (Figure 1f), at $\Delta E = 4.8 \text{ eV}$ is MnO_2 , indicating the successful synthesis of MnO_2 particles.

Figure 2a shows the SEM images of h-BNNs, and we observed that the ultrasonically stripped h-BNNs showed a flat lamellar shape with thin lamellae, while in the SEM of the composite MnO_2 @h-BNNs (Figure 2b), the presence of sphere-like MnO_2 on the surface of h-BNNs could be clearly observed. This indicates that the ultrasonically stripped h-BNNs did not destroy its lamellar structure. The hydrothermally synthesized MnO_2 particles successfully covered the surface of the nanosheets. The TEM images of the composite MnO_2 @h-BNNs material in Figure 2c,d show that the sphere-like MnO_2 nanoparticles were generated and distributed between the lamellae of h-BNNs with lattice spacing of 0.24 nm and 0.21 nm corresponding to the (11-1) face of MnO_2 nanoparticles and the (100) face of

h-BNNs, respectively. The MnO_2 @h-BNNs diffractograms are consistent with the (11-1) reflections of MnO_2 and the (100) and (110) reflections of h-BN, which further confirms that the composite MnO_2 @h-BNNs were successfully synthesized.

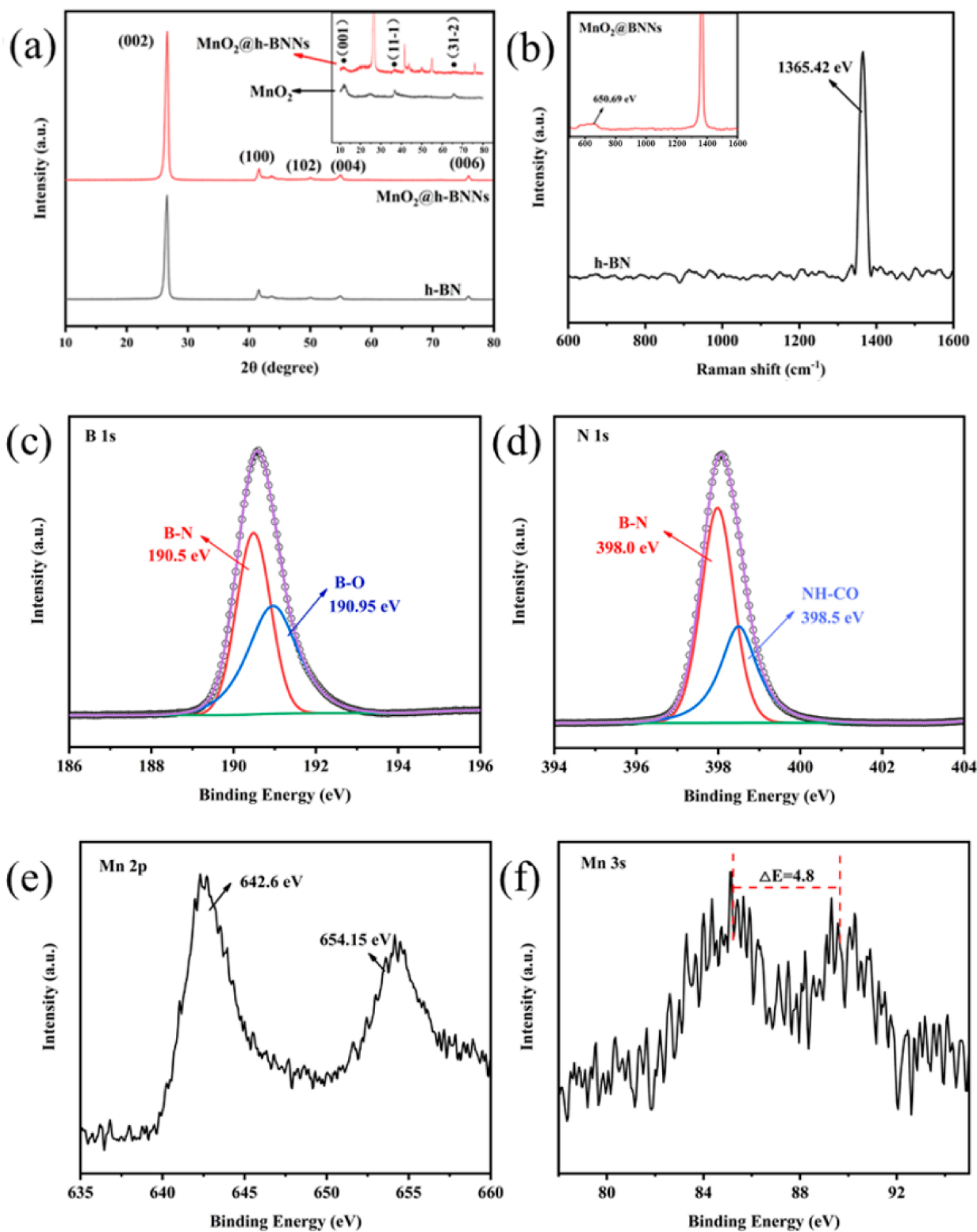


Figure 1. XPS fits of (a) XRD plots, (b) Raman spectra, and (c) B 1s, (d) N 1s, (e) Mn 2p, (f) Mn 3s of h-BN, and MnO_2 @h-BNNs.

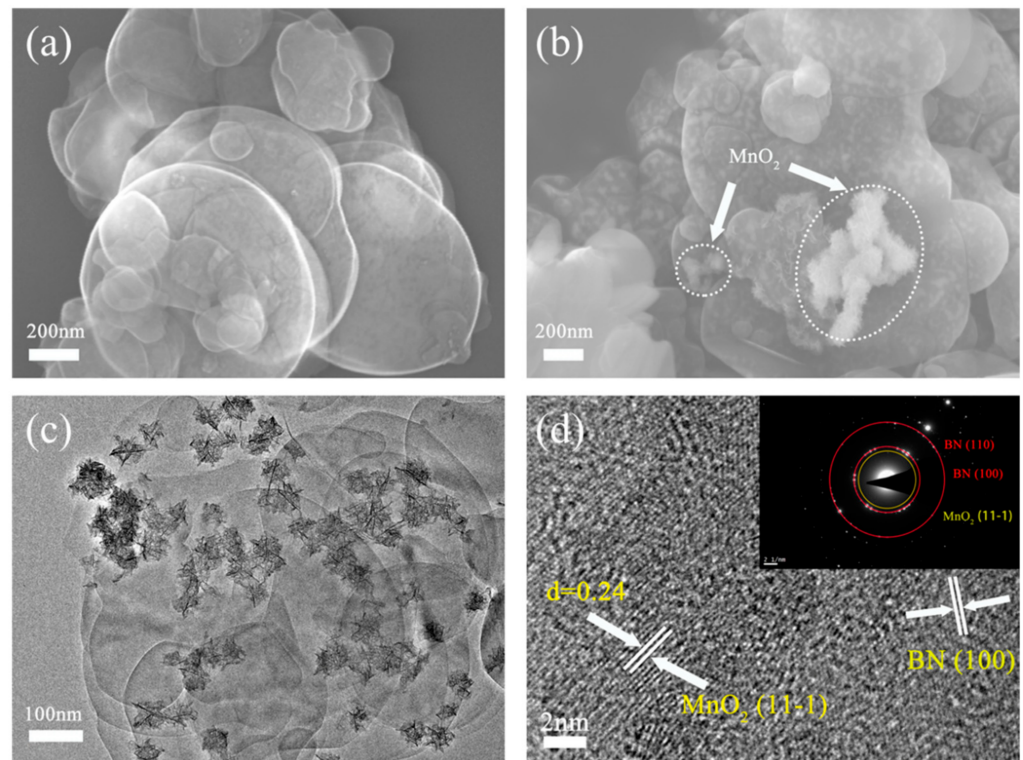


Figure 2. SEM images of BNNs (a) and MnO_2 @h-BNNs (b) and TEM images of MnO_2 @h-BNNs (c,d).

3.2. Tribological Properties

In the constant-temperature test, Figure 3a,b show the FC curves and average friction coefficients (Avg. FC), respectively, of MnO_2 @h-BNNs additives with different additive contents. From Figure 3a, it can be seen that as the time proceeds, the values gradually smooth out after the break-in period, and the friction curve containing MnO_2 @h-BNNs additive has a clear decreasing trend. The FC curve decreased most significantly when the concentration of the additive was 0.25 wt%. At this time, the average Avg. FC was at the lowest value (Avg. FC = 0.0794, 42.40% lower), and the friction reduction effect was the most obvious, as shown in Figure 3b. When the additive content was less than 0.25 wt%, the Avg. FC (Avg. FC = 0.083, 39.54% reduction) was higher than the value of the 0.25 wt% oil sample, which may be because it had less additive content and there was not enough material to form a lubricating film in the contact area of mechanical parts [39]. It is noteworthy that the FC curve increased when the additive concentration was 0.5%, while the Avg. FC (Avg. FC = 0.0795, 42.33% reduction) was also higher than 0.25 wt%. This may be due to the higher concentration of the MnO_2 @h-BNNs additive, which can form a protective film in the friction contact area faster, resulting in a shorter break-in period and a faster stabilization of the FC curve. However, as analyzed in Section 3.4 on dispersion stability, too high a concentration of nanoparticles tends to lead to the formation of larger aggregates. Nanoadditives lose their small size effect due to the formation of larger particles, which accumulate in the friction contact zone and lead to abrasive wear [40,41].

Figure 4a,b shows the friction test curves and the Avg. FC for different additives. During the friction test, the FC curves of the PAO6 oil samples with other additives were all reduced to different degrees compared with the PAO6 base oil (Figure 4a). The FC of PAO6 oil showed a peak FC at the beginning of the test (0–250 s), and the Avg. FC value was maintained at about 0.14 after the break-in period. In contrast, for the lubricant with the addition of 3% Span80 dispersant, 0.25 wt% h-BN s, 0.25 wt% BNNs, and MnO_2 @h-BNNs to PAO6, the FC curve gradually decreased with the extension of the test time, and the friction reduction effect was revealed. Among them, the oil samples with the 0.25 wt% MnO_2 @h-BNNs additive showed a more obvious friction reduction effect than the other

samples, and the FC reduced to about 0.045 at the later stage, which may be due to the synergistic effect of the doped MnO_2 particles and h-BNNs in substantially reducing the frictional wear [42]. Figure 4b shows the Avg. FC of the oil samples; the FC of the 0.25 wt% MnO_2 @h-BNNs additive was also the smallest, and its Avg. FC was reduced from 0.138 to 0.079 for pure oil, which was 42.4% lower. The above results show that the dispersant Span80 helps to reduce friction, and the friction reduction effect of MnO_2 @h-BNNs is better than that of h-BN powder when coblended with h-BN powder or the MnO_2 @h-BNNs lubricant additive dispersed in the base oil.

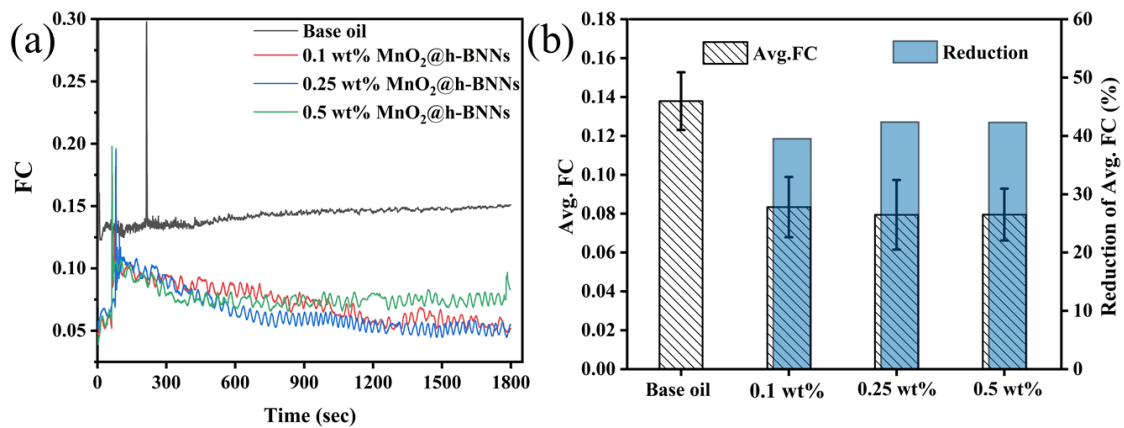


Figure 3. FC curves (a) and Avg. FC (b) for different contents of MnO_2 @h-BNNs additives.

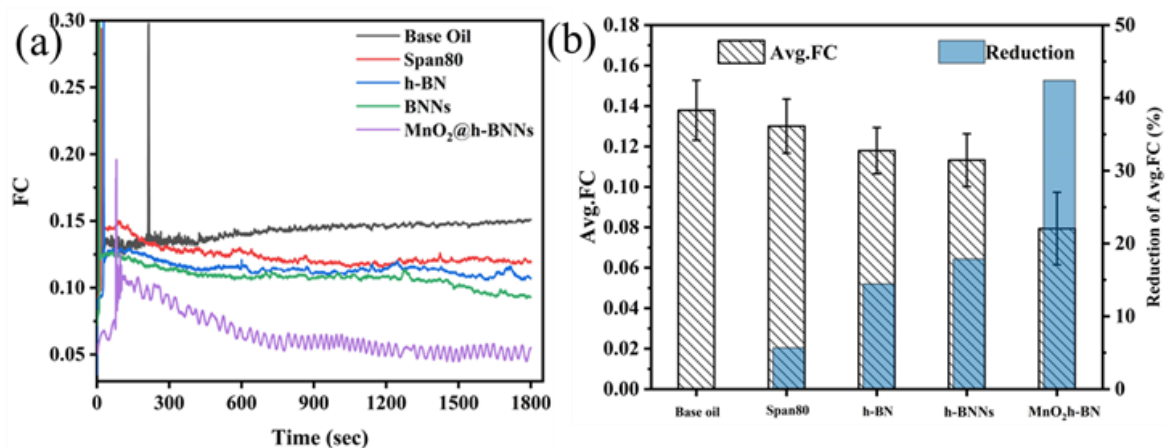


Figure 4. FC curves (a) and Avg. FC (b) of oil samples with different compositions.

The antiwear performance of MnO_2 @h-BNNs nanoadditives blended with base oils can be evaluated based on the wear scar diameter (WSD). The wear scar diameter depends on the magnitude of the applied load and the load-carrying capacity of the lubricant. A large WSD indicates a high wear rate and a low lubricant carrying capacity, while the opposite indicates a low wear rate and a high lubricant carrying capacity. The WSDs of the three bottom spheres were measured using optical microscopy, and the average wear scar diameters of the oil samples with different concentrations of MnO_2 @h-BNNs nanoadditives are shown in Figure 5a. The results confirm that the addition of MnO_2 @h-BNNs additives effectively improved the antiwear performance compared with the base oil, with the best antiwear performance at the concentration of 0.25 wt%, which was about 11.19% lower. Additionally, the antiwear performance of the lubricant decreased instead with the increase in the additive content. This is due to the high surface energy of the nanoadditives. When the concentration of additive is too high, they form high intermolecular force and tend to agglomerate into larger particles, which will cause abrasive wear in the friction process. Figure 5b shows the WSD of different additives; it can be seen that the addition of Span80

contributed to less wear and the WSD of steel balls became larger after the addition of solid additives. Thus, compared with other additives, the MnO_2 @h-BNNs additive has the best antiwear effect.

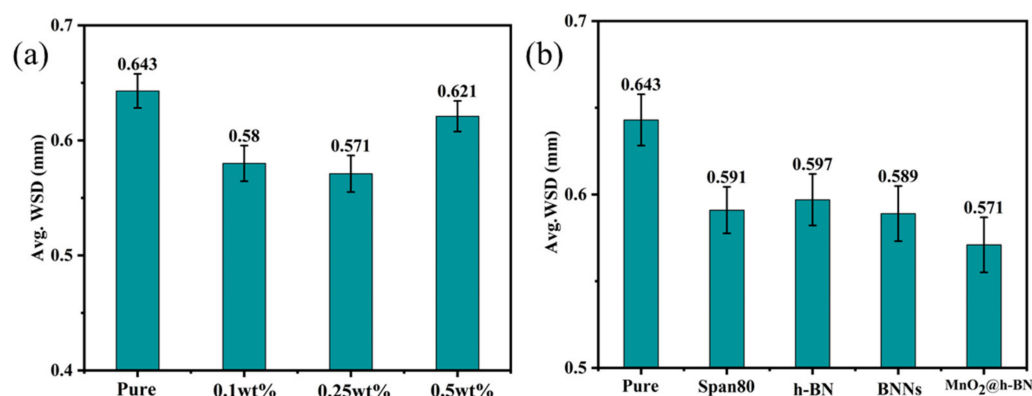


Figure 5. (a) WSD of different concentrations of MnO_2 @h-BNNs and (b) WSD of different additives.

The results show that both h-BN and MnO_2 @h-BNNs nanoadditives can improve the friction reduction and antiwear properties of the oil samples, among which the lubrication performance of MnO_2 @h-BNNs nanomaterials was better than that of h-BN, which is probably due to the synergistic lubrication effect of MnO_2 particles and h-BNNs. The h-BNNs has thin lamellae, which can continuously enter the friction surface and adsorb on the friction surface to form a lubricating film. The MnO_2 particles are modified between the h-BNNs, which effectively prevent the agglomeration of the nanoflakes and make the h-BNNs slip more easily during the friction process. At the same time, the small size of MnO_2 particles allows them to enter the friction surface, fill micropits and scratches, and repair wear marks as well as prevent further deepening of wear.

3.3. Analysis of Wear Interface

To further reveal the frictional wear behavior, the wear traces were investigated using SEM, laser confocal, and XPS with a MnO_2 @h-BNNs additive as an example. Figure 6a–d show the optical scan images of the wear traces of the MnO_2 @h-BNNs samples after the 30 min test. The wear surface of the steel balls lubricated with PAO6 base oil was very rough, with obvious micropits as well as long plow grooves (Figure 6a). In contrast, after adding the MnO_2 @h-BNNs additive, the wear surface of the steel balls became flatter, with fewer micropits and furrows and only a few shallow and slight grooves, indicating that the lubrication condition was significantly improved and the frictional wear was greatly reduced. Analyzing the reason, the wear surface of steel balls lubricated with oil samples of MnO_2 @h-BNNs additives could be observed to be covered with thin layers of wrinkled flakes, which may be due to the applied load on MnO_2 @h-BNNs, particle collapse, and flake breakage finally forming a protective layer on the wear surface. According to studies in the literature [43,44], it is known that the thin layer of wrinkling caused by sliding friction is more pronounced as the number of layers deposited on the friction surface increases, and thus the friction decreases as the thin layer is observed on the wear surface. However, as the additive concentration increased, a single deeper groove appeared on the wear surface of the steel balls. This is due to the high tendency of highly concentrated nanoparticles to aggregate, which makes it difficult for the MnO_2 @h-BNNs additive to enter the frictional contact surface to form a continuous and uniform antiwear layer. To further confirm the composition of the surface of the steel ball wear marks, EDS was used for analysis, as shown in Figure 6e–g. Fe, Cr, B, N, and trace amounts of Mn elements were present on the surface of the steel balls. This indicates that MnO_2 @h-BNNs act on the wear surface of the steel balls, thus reducing the frictional wear.

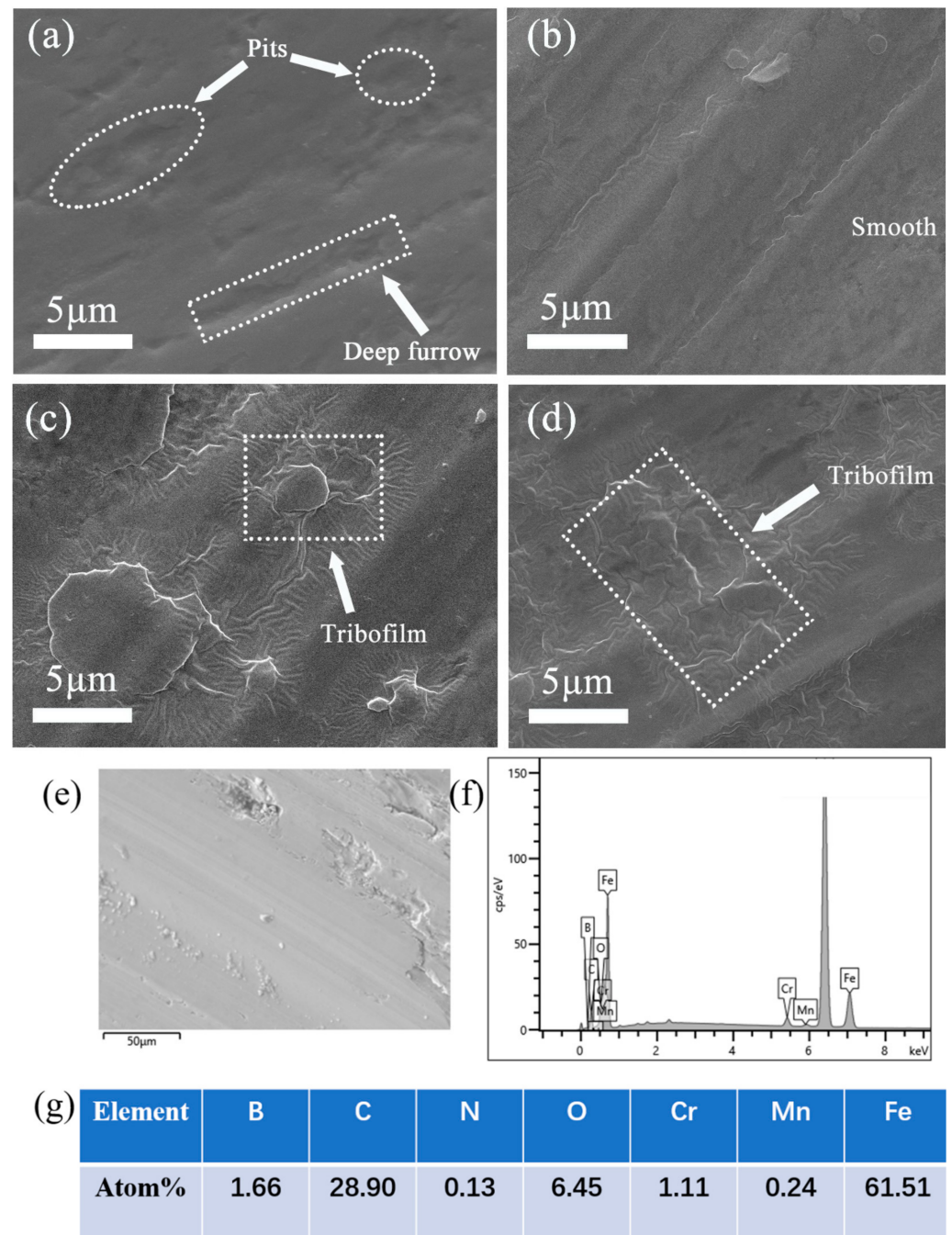


Figure 6. SEM images of the wear surface of (a) PAO6, (b) 0.1 wt%, (c) 0.25 wt%, and (d) 0.5 wt% steel balls. (e–g) EDS of 0.25 wt%.

A three-dimensional image construction and line scan of the wear surface of the steel ball were performed using a laser confocal technique. As shown in Figure 7a, the wear surface of the steel balls lubricated with PAO6 base oil is extremely rough with many wide and deep grooves, and a single deep scratch can be observed on the left side of the steel ball, which could be due to the abrasive wear caused by the shedding of iron chips. The steel balls lubricated with the PAO6 base oil have the largest diameter of wear marks, and the addition of the MnO₂@h-BNNs nanoadditive to the oil samples resulted in smaller, shallower scratches and grooves and smaller diameter of wear marks on the wear surface of the steel balls, which is consistent with the WSD values of the steel balls in Figure 5a. However, Figure 8 shows the contour lines of wear marks on the surface of the steel balls after lubrication with different concentrations, and it can be noticed that

the surface of the 0.1 wt% MnO₂@h-BNNs/PAO6-lubricated steel ball is flatter, and as the additive content increased, the same deep scratches appeared at the wear interface as in the original sample, as shown in Figure 7b–d. This may be due to the increased viscosity caused by the increased nanoadditive content (Section 3.5), which prevents the iron filings from leaving the frictional contact surface and thus leads to wear of the abrasive particles.

Table 1 shows the wear volume of the lubricants with different contents of MnO₂@BNNs/PAO6. The average wear volume of PAO6 was 28,763.738 μm³. The addition of the MnO₂@BNNs additive reduced the average wear volume of the steel balls, with the smallest average wear volume being 11,004.551 μm³ for 0.1 wt% MnO₂@BNNs. As the MnO₂@BNNs content increases, the average wear volume increases, which is an increase in wear volume due to the appearance of deep scratches, in agreement with the analysis of the 3D morphology.

XPS analysis was performed to investigate the chemical composition of the wear surface of steel balls lubricated with 0.25 wt% MnO₂@h-BNNs oil samples and to explore the lubrication mechanism of the MnO₂@h-BNNs additive. Figure 9a shows the full spectrum of XPS on the steel ball surface. The presence of C, O, Fe, B, N, and Mn on the wear surface of the steel ball after the addition of the nanoadditive is consistent with the SEM-EDS results of the steel ball's wear surface. The difficulty in detecting the signal of B 1s on the steel ball surface is due to the low sensitivity of B 1s. Figure 9a shows the Fe 2p spectra with FeS, Fe₃O₄, FeOOH, and Fe₂O₃ signals appearing at binding energies of 707.28 eV, 710.05 eV, 711.24 eV, and 724.99 eV, respectively [45–47], which may be due to the oxidation reaction of Fe during the friction process. It is noteworthy that the appearance of FeS may be due to the inhomogeneous composition of the steel balls, where the S element of the matrix reacts with Fe to produce FeS under a high temperature and pressure [47]. Figure 9c,d show the N 1s and Mn 2p spectra of the steel ball surfaces, respectively. In comparison with the XPS spectra of MnO₂@BNNs before the test, the N 1s peak reveals the presence of two forms: the peak at 399.79 eV belongs to organic nitrogen and the peak at 397.79 eV belongs to B-N bonding, mainly from h-BNNs in additives. Trace amounts of Mn elements were also found on the wear surface of the steel balls, and the Mn 2p spectrum shows a 9.66 eV separation between the Mn 2p 1/2 peak and the Mn 2p 3/2 peak, which is in general agreement with the peaks of MnO₂@BNNs. Combining the above analysis results with the SEM morphology of the steel ball wear marks and the SEM-EDS test results, it was confirmed that the h-BNNs and MnO₂ particles in the lubricant acted on the friction surface during the sliding process. The MnO₂@h-BNNs additive is easily adsorbed on the friction surface during the friction process due to its large surface energy, forming an adsorption film. When the nanoadditive collapses under the action of external force, MnO₂ particles enter the wear surface to fill the micropits, and h-BNNs enter the contact area to lay flat on the friction contact surface and oxidize to form a protective film under a high temperature and pressure, thus reducing friction and wear. The protective film formed on the friction subsurface prevents the further generation of wear, separates the friction contact surface, greatly improves the lubrication performance, and protects the surface from pit erosion.

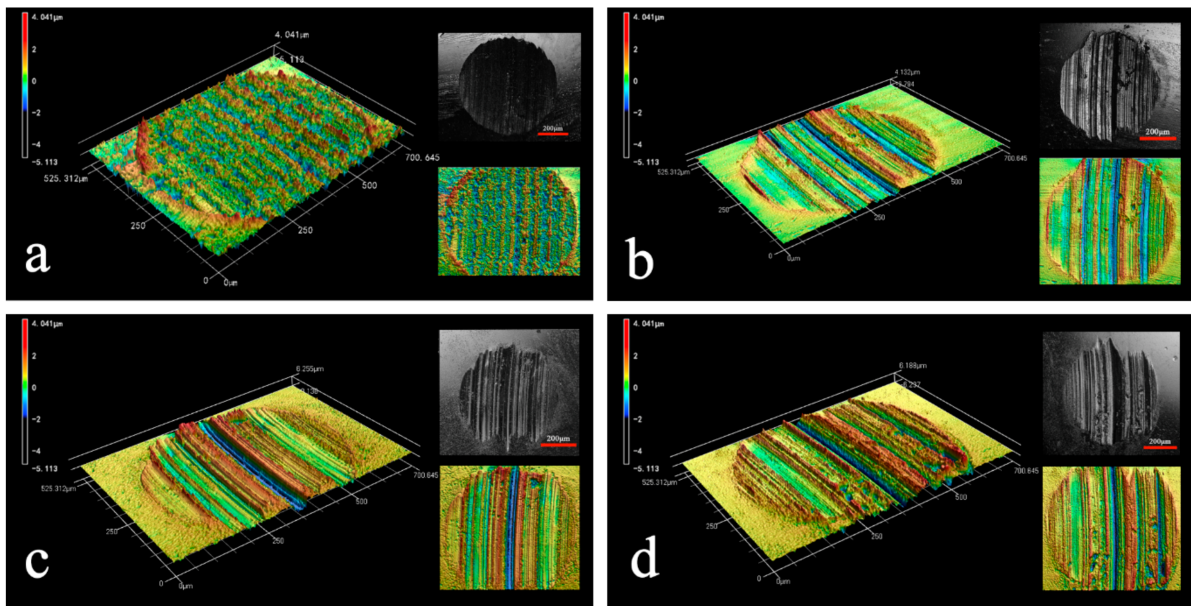


Figure 7. (a) PAO6, (b) 0.1 wt%, (c) 0.25 wt%, and (d) 0.5 wt% laser confocal.

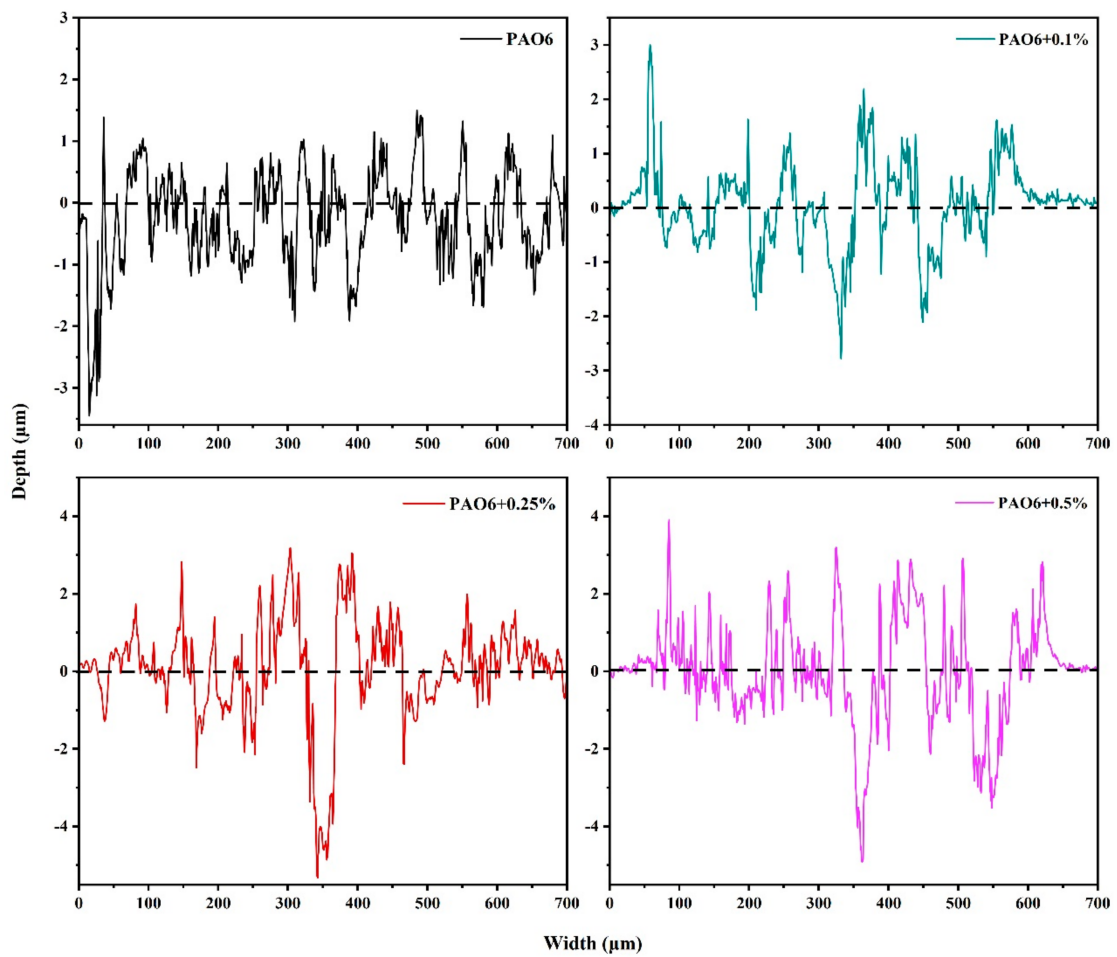
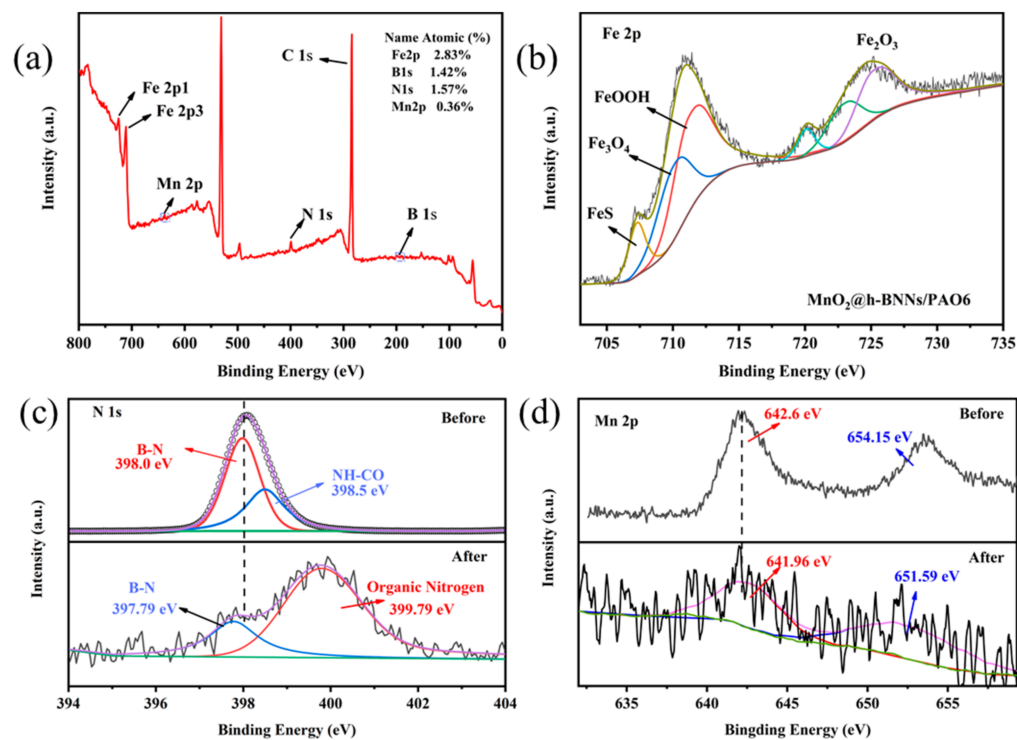


Figure 8. Contours of wear marks of MnO₂@h-BNNs.

Table 1. Wear volume of lubricating oil with different contents of MnO₂@BNNs/PAO6.

Sample	Mean Wear Volume (μm^3)
PAO6	28,763.738
0.1 wt% MnO ₂ @BNNs	11,004.551
0.25 wt% MnO ₂ @BNNs	20,887.380
0.5 wt% MnO ₂ @BNNs	24,573.150

**Figure 9.** XPS spectrum: (a) full spectrum, (b) Fe 2p, (c) N 1s, and (d) Mn 2p on the surface of steel ball.

3.4. Dispersion Stability

In tribological studies, the dispersion stability of lubricating additives is considered to be the most critical factor in their practical application. According to the principle of similar phase solubility, the nanoadditive was dispersed in petroleum ether, and the dispersion of the samples was analyzed by observing the morphology of the additive deposited on the silicon wafer (Figure 10a,b). It can be found that the sample without dispersant undergoes agglomeration and forms larger particles, while the sample with Span80 added distributes smaller particles on the wafer without obvious agglomeration. It indicates that Span80 can effectively disperse the nanoadditive. The stability of the samples was further verified by UV-Vis spectrophotometer by dispersing 0.1 wt% of MnO₂@h-BNNs into the base oil with the addition of Span80 dispersant as a comparison sample. As shown in Figure 11, the change in transmittance with time reflects the stability of particle dispersion in solution. The transmission rate of the oil sample without dispersant decreased rapidly with the extension of settling time, while the oil sample with dispersant added, the MnO₂@h-BNNs nanoadditive, was able to maintain a better dispersion stability.

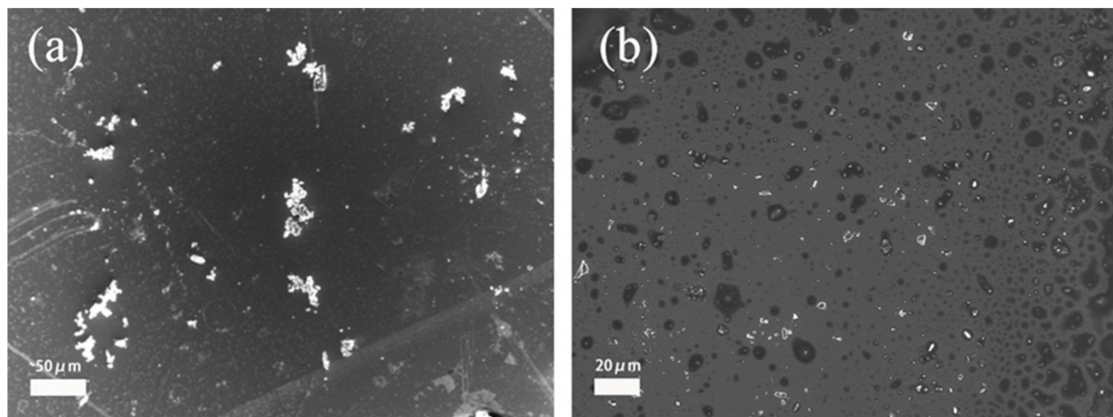


Figure 10. SEM plots of (a) MnO₂@h-BNNs without Span80 and (b) MnO₂@h-BNNs with Span80 dispersion at a content of 0.1%.

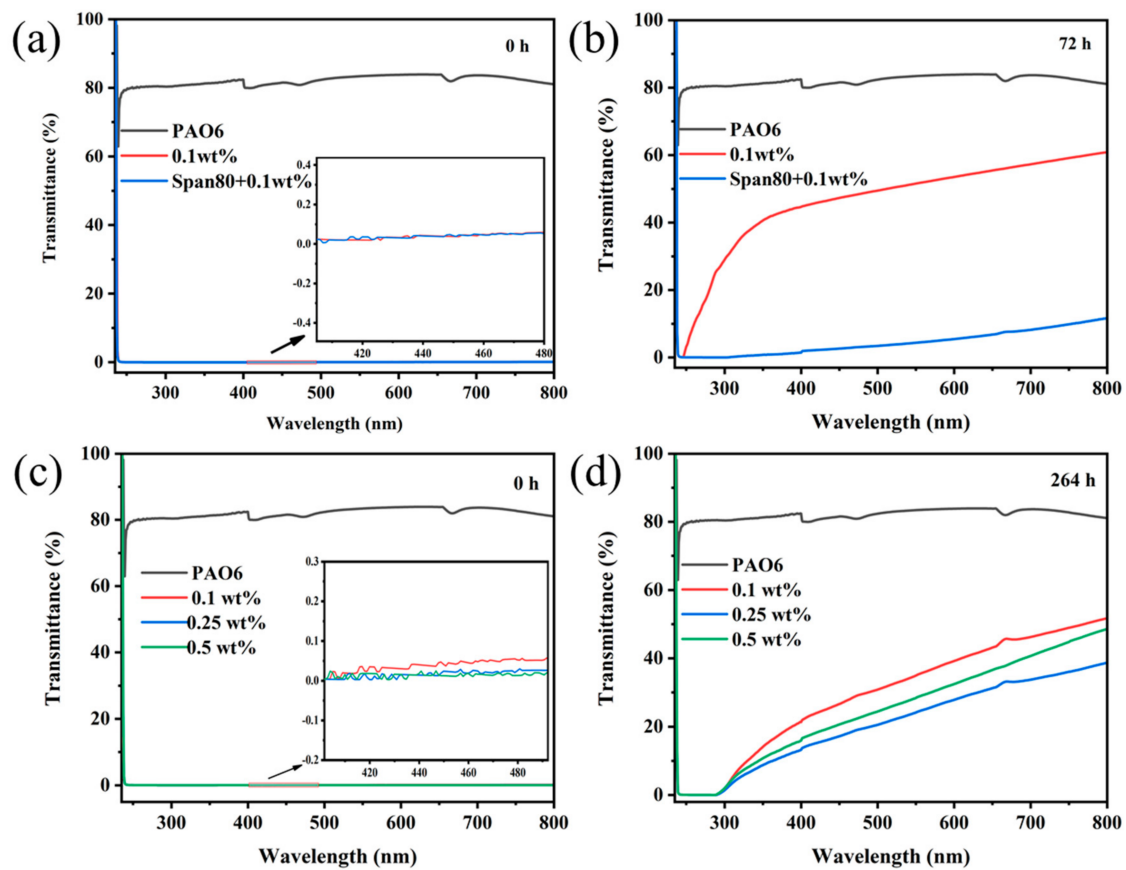


Figure 11. UV spectra of Span80-dispersed 0.1 wt% MnO₂@h-BNNs/PAO6 lubricant (a,b) and different concentrations of MnO₂@h-BNNs/PAO6 (c,d).

3.5. Viscosity

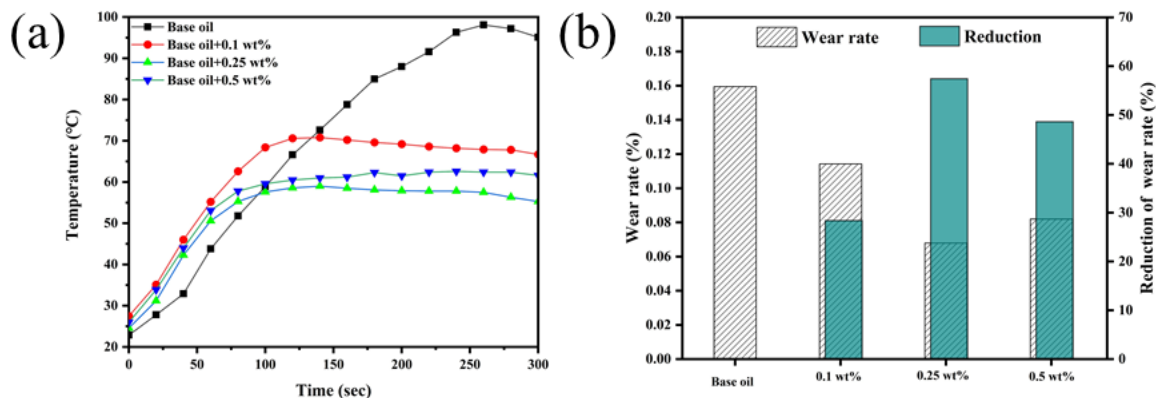
In order to better study the effect of additives on the physical properties of PAO6 oil and evaluate the comprehensive performance of MnO₂@h-BNNs, the viscosity of PAO6, Span80, and different concentrations of MnO₂@h-BNNs/PAO6 were tested at 100 °C using a viscometer (CP-3000). As shown in Table 2, the viscosity of PAO6 base oil was 6.026 mPa·s at 100 °C, while the viscosity of Span80 was larger, reaching about 26.14 mPa·s. After adding 3% Span80 and different concentrations of MnO₂@h-BNNs, the viscosity of the oil samples gradually increased with a maximum difference of 0.594.

Table 2. Viscosity of oil samples at 100 °C.

Sample	Viscosity (mPa·s)
PAO6	6.026
Span80	26.14
3% Span80/0.1 wt% MnO ₂ @h-BNNs/PAO6	6.371
3% Span80/0.25 wt% MnO ₂ @h-BNNs/PAO6	6.567
3% Span80/0.5 wt% MnO ₂ @h-BNNs/PAO6	6.620

3.6. Variable-Temperature Test Analysis

In order to investigate the oil temperature variation and wear rate of the MnO₂@h-BNNs nanoadditive in actual operation, a 280 W pointer-type standard lubricant antiwear tester was used to test the antiwear performance of the additive under constant load and constant time (980 N, 5 min). Figure 12a shows the change curve of oil temperature during operation. The oil temperature of PAO6 base oil reached 98.1 °C at about 250 s and then stabilized. The oil temperature of oil containing MnO₂@h-BNNs was higher than that of base oil in the first 100 s, while all stabilized after 100 s, when the oil samples with 0.1 wt%, 0.25 wt%, and 0.5 wt% additives reached 68.4 °C, 57.6 °C, and 59.6 °C, respectively, with a lower temperature plateau than that of base oil. These results indicate that the MnO₂@h-BNNs nanoadditive has better thermal conductivity in oil, and its rapid temperature rise rate and the early appearance of temperature plateau can effectively control the oil temperature rise, with the best content being 0.25 wt%. The antiwear effect of the MnO₂@h-BNNs additive in the variable-temperature test was evaluated by comparing the reduction in steel bead mass before and after the test. The results show that the MnO₂@h-BNNs nanoadditive can significantly reduce the wear rate. As shown in Figure 12b, the lowest wear rate of 0.25 wt% sample was about 0.067%, which was 57.4% lower compared to the base oil. The wear rate results are consistent with the oil temperature change curve; the lower the temperature at which the oil sample tends to stabilize, the smaller the viscosity change, thus reducing the wear.

**Figure 12.** (a) Oil temperature change curve and (b) wear rate.

3.7. Mechanism Analysis

Based on all the above results, nanoparticles filling micropits and the formation process of boron-based friction film are proposed to explain the lubrication mechanism of MnO₂@h-BNNs additives, as shown in Figure 13. Due to the nanoscale of MnO₂@h-BNNs, it can be easily transferred to the friction surface contact gap continuously with liquid oil during the friction process. At a high temperature and pressure (100 °C, 392 N), the MnO₂@h-BNNs additive enters the friction contact surface and deposits and adheres to the friction surface to form a lubricating film. Under the action of mechanical force and heat, the iron on the surface of the steel balls undergoes an oxidation reaction and forms a friction protection film with the nanoadditives deposited and adsorbed on the surface. The lubrication performance of MnO₂@h-BNNs is better than that of h-BN, which is mainly

due to the synergistic lubrication between MnO_2 particles and h-BNNs. MnO_2 particles on the surface of h-BNNs can act as balls during the friction process, and the adsorption and deposition of two-dimensional materials on the friction surface can effectively reduce the friction. Meanwhile, the small size effect of MnO_2 particles allows them to enter the friction surface and fill micropits and scratches, repairing wear as well as preventing further deepening of wear, as confirmed by XPS and SEM-EDS tests. The boron-containing friction film can avoid rough contact and reduce frictional wear. In addition, h-BNNs have high thermal stability, which helps to improve the loading capacity under severe conditions. This boron-containing friction film can exist at a high temperature and high normal force, which can effectively protect the friction surface and reduce wear. It could be confirmed that h-BNN composites effectively avoid the direct contact of the friction surface, improve the antiwear performance of the friction substrate, and reduce the surface pitting.

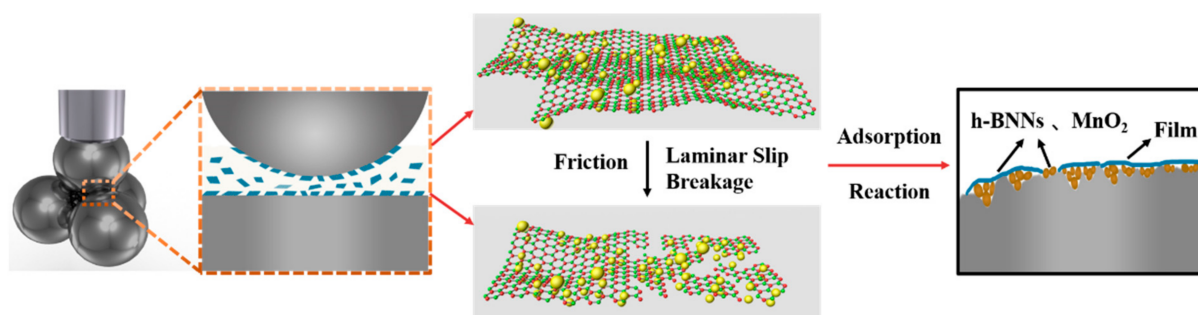


Figure 13. Schematic diagram of lubrication model of MnO_2 @h-BNNs additive in PAO6 oil.

4. Conclusions

MnO_2 @h-BNNs nanoadditives were prepared by ultrasonic exfoliation of h-BN and hydrothermal encapsulation of MnO_2 particles. The addition of trace amounts of MnO_2 @h-BNNs nanomaterials to PAO6 oil in the constant-temperature test resulted in an extremely low FC and wear rate. Compared with PAO6 base oil, the addition of 0.25% MnO_2 @h-BNNs to PAO6 base oil reduced the steel–steel contact FC by 42% and the wear rate by 11.19%. In the variable-temperature test, the nanoadditive could effectively control the increase in oil temperature with good thermal stability, and the wear rate was reduced by about 57.4% compared with PAO6 base oil. The excellent tribological properties of MnO_2 @h-BNNs are due to the deposition of nanomaterials, which form a physical protective film at the friction interface. At the same time, the chemical reaction at the friction interface leads to the formation of boron-based films. The formation of the friction film is responsible for its extremely low FC and excellent wear resistance. In addition, MnO_2 promotes the slippage and collapse of h-BNNs, which in turn promotes the lubrication effect.

Author Contributions: Conceptualization, X.C. and W.C.; methodology, X.C.; software, S.Y. and Z.Y.; validation, X.C. and W.C.; formal analysis, L.Z.; investigation, W.C.; resources, X.C.; data curation, M.Z.; writing—original draft preparation, X.C.; writing—review and editing, O.O. and K.T.; visualization, X.C.; supervision, N.W.; project administration, N.W.; funding acquisition, Y.Z. All authors have read and agreed to the published version of the manuscript.

Funding: National Natural Science Foundation (grant no.: 51972068).

Institutional Review Board Statement: Not applicable.

Informed Consent Statement: Not applicable.

Data Availability Statement: Not applicable.

Acknowledgments: This work was supported by the grants from the Key Laboratory of New Processing Technology for Nonferrous Metals and Materials. to the authors also thank FullerStar Ltd. for providing the related materials.

Conflicts of Interest: The authors declare no conflict of interest.

References

1. Holmberg, K.; Andersson, P.; Nylund, N.-O.; Mäkelä, K.; Erdemir, A. Global energy consumption due to friction in trucks and buses. *Tribol. Int.* **2014**, *78*, 94–114. [[CrossRef](#)]
2. Holmberg, K.; Erdemir, A. Influence of tribology on global energy consumption, costs and emissions. *Friction* **2017**, *5*, 263–284. [[CrossRef](#)]
3. Holmberg, K.; Kivikytö-Reponen, P.; Härkisaari, P.; Valtonen, K.; Erdemir, A. Global energy consumption due to friction and wear in the mining industry. *Tribol. Int.* **2017**, *115*, 116–139. [[CrossRef](#)]
4. Sengupta, S.; Murmu, M.; Mandal, S.; Hirani, H.; Banerjee, P. Competitive corrosion inhibition performance of alkyl/acyl substituted 2-(2-hydroxybenzylideneamino)phenol protecting mild steel used in adverse acidic medium: A dual approach analysis using FMOs/ molecular dynamics simulation corroborated experimental findings. *Colloids Surf. A Physicochem. Eng. Asp.* **2021**, *617*, 126314. [[CrossRef](#)]
5. Luo, J.; Zhou, X. Superlubricative engineering—Future industry nearly getting rid of wear and frictional energy consumption. *Friction* **2020**, *8*, 643–665. [[CrossRef](#)]
6. Xiao, H.; Liu, S. 2D nanomaterials as lubricant additive: A review. *Mater. Des.* **2017**, *135*, 319–332. [[CrossRef](#)]
7. Uzoma, P.C.; Hu, H.; Khadem, M.; Penkov, O.V. Tribology of 2D Nanomaterials: A Review. *Coatings* **2020**, *10*, 897. [[CrossRef](#)]
8. Nosonovsky, M.; Bhushan, B. Green tribology: Principles, research areas and challenges. *Philos. Trans. A Math. Phys. Eng. Sci.* **2010**, *368*, 4677–4694. [[CrossRef](#)]
9. Senatore, A.; D’Agostino, V.; Petrone, V.; Ciambelli, P.; Sarno, M. Graphene Oxide Nanosheets as Effective Friction Modifier for Oil Lubricant: Materials, Methods, and Tribological Results. *ISRN Tribol.* **2013**, *2013*, 425809. [[CrossRef](#)]
10. Zheng, D.; Wu, Y.P.; Li, Z.Y.; Cai, Z.B. Tribological properties of WS₂/graphene nanocomposites as lubricating oil additives. *RSC Adv.* **2017**, *7*, 14060–14068. [[CrossRef](#)]
11. Wu, X.; Gong, K.; Zhao, G.; Lou, W.; Wang, X.; Liu, W. Mechanical synthesis of chemically bonded phosphorus–graphene hybrid as high-temperature lubricating oil additive. *RSC Adv.* **2018**, *8*, 4595–4603. [[CrossRef](#)]
12. Rapoport, L.; Fleischer, N.; Tenne, R. Applications of WS₂(MoS₂) inorganic nanotubes and fullerene-like nanoparticles for solid lubrication and for structural nanocomposites. *J. Mater. Chem.* **2005**, *15*, 1782–1788. [[CrossRef](#)]
13. Xu, Y.; Hu, E.; Hu, K.; Xu, Y.; Hu, X. Formation of an adsorption film of MoS₂ nanoparticles and dioctyl sebacate on a steel surface for alleviating friction and wear. *Tribol. Int.* **2015**, *92*, 172–183. [[CrossRef](#)]
14. Hou, X.; Jiang, H.; Ali, M.K.A.; Liu, H.; Su, D.; Tian, Z. Dispersion behavior assessment of the molybdenum disulfide nanomaterials dispersed into poly alpha olefin. *J. Mol. Liq.* **2020**, *311*, 113303. [[CrossRef](#)]
15. Bondarev, A.V.; Fraile, A.; Polcar, T.; Shtansky, D.V. Mechanisms of friction and wear reduction by h-BN nanosheet and spherical W nanoparticle additives to base oil: Experimental study and molecular dynamics simulation. *Tribol. Int.* **2020**, *151*, 106493. [[CrossRef](#)]
16. Chen, J.; Chen, J.; Wang, S.; Sun, Q.; Cheng, J.; Yu, Y.; Yang, J. Tribological properties of h-BN matrix solid-lubricating composites under elevated temperatures. *Tribol. Int.* **2020**, *148*, 106333. [[CrossRef](#)]
17. Tang, G.; Su, F.; Xu, X.; Chu, P.K. 2D black phosphorus dotted with silver nanoparticles: An excellent lubricant additive for tribological applications. *Chem. Eng. J.* **2020**, *392*, 123631. [[CrossRef](#)]
18. Wang, Q.; Hou, T.; Wang, W.; Zhang, G.; Gao, Y.; Wang, K. Tribological behavior of black phosphorus nanosheets as water-based lubrication additives. *Friction* **2021**, *10*, 374–387. [[CrossRef](#)]
19. Weng, Q.; Wang, X.; Wang, X.; Bando, Y.; Golberg, D. Functionalized hexagonal boron nitride nanomaterials: Emerging properties and applications. *Chem. Soc. Rev.* **2016**, *45*, 3989–4012. [[CrossRef](#)]
20. Niu, Z.B.; Chen, F.; Xiao, P.; Li, Z.; Pang, L.; Li, Y. Effect of h-BN addition on friction and wear properties of C/C-SiC composites fabricated by LSI. *Int. J. Appl. Ceram. Technol.* **2021**, *19*, 108–118. [[CrossRef](#)]
21. Wang, L.; Gong, P.; Li, W.; Luo, T.; Cao, B. Mono-dispersed Ag/Graphene nanocomposite as lubricant additive to reduce friction and wear. *Tribol. Int.* **2020**, *146*, 106228. [[CrossRef](#)]
22. Guo, Y.; Zhou, X.; Lee, K.; Yoon, H.C.; Xu, Q.; Wang, D. Recent development in friction of 2D materials: From mechanisms to applications. *Nanotechnology* **2021**, *32*, 312002. [[CrossRef](#)]
23. Gupta, M.K.; Bijwe, J.; Padhan, M. Role of size of hexagonal boron nitride particles on tribo-performance of nano and micro oils. *Lubr. Sci.* **2018**, *30*, 441–456. [[CrossRef](#)]
24. Liu, C.; Tang, G.; Su, F.; Xu, X.; Li, Z. Functionalised h-BN as an effective lubricant additive in PAO oil for MoN coating sliding against Si₃N₄ball. *Lubr. Sci.* **2020**, *33*, 33–42. [[CrossRef](#)]
25. Raina, A.; Irfan Ul Haq, M.; Anand, A.; Mohan, S.; Kumar, R.; Jayalakshmi, S.; Arvind Singh, R. Nanodiamond particles as secondary additive for polyalphaolefin oil lubrication of steel-aluminium contact. *Nanomaterials* **2021**, *11*, 1438. [[CrossRef](#)]
26. Shukla, N.; Verma, D.K.; Singh, A.K.; Kumar, B.; Kavita; Rastogi, R.B. Ternary Composite of Methionine-Functionalized Graphene Oxide, Lanthanum-Doped Yttria Nanoparticles, and Molybdenum Disulfide Nanosheets for Thin-Film Lubrication. *ACS Appl. Nano Mater.* **2020**, *3*, 8012–8026. [[CrossRef](#)]
27. Rajendhran, N.; Palanisamy, S.; Periyasamy, P.; Venkatachalam, R. Enhancing of the tribological characteristics of the lubricant oils using Ni-promoted MoS₂ nanosheets as nano-additives. *Tribol. Int.* **2018**, *118*, 314–328. [[CrossRef](#)]
28. Wu, H.; Yin, S.; Du, Y.; Wang, L.; Yang, Y.; Wang, H. Alkyl-Functionalized Boron Nitride Nanosheets as Lubricant Additives. *ACS Appl. Nano Mater.* **2020**, *3*, 9108–9116. [[CrossRef](#)]

29. Lu, Z.; Cao, Z.; Hu, E.; Hu, K.; Hu, X. Preparation and tribological properties of WS₂ and WS₂/TiO₂ nanoparticles. *Tribol. Int.* **2019**, *130*, 308–316. [[CrossRef](#)]
30. Chen, B.; Zhang, M.; Li, X.; Dong, Z.; Jia, Y.; Li, C. Tribological properties of epoxy-based self-lubricating composite coating enhanced by 2D/2D h-BN/MoS₂ hybrid. *Prog. Org. Coat.* **2020**, *147*, 105767. [[CrossRef](#)]
31. Zhao, J.; Huang, Y.; He, Y.; Shi, Y. Nanolubricant additives: A review. *Friction* **2020**, *9*, 891–917. [[CrossRef](#)]
32. Liñeira del Río, J.M.; López, E.R.; Fernández, J. Tribological properties of graphene nanoplatelets or boron nitride nanoparticles as additives of a polyalphaolefin base oil. *J. Mol. Liq.* **2021**, *333*, 115911. [[CrossRef](#)]
33. Murmu, M.; Sengupta, S.; Pal, R.; Mandal, S.; Murmu, N.C.; Banerjee, P. Efficient tribological properties of azomethine-functionalized chitosan as a bio-lubricant additive in paraffin oil: Experimental and theoretical analysis. *RSC Adv.* **2020**, *10*, 33401–33416. [[CrossRef](#)]
34. Subramanian, V.; Zhu, H.; Wei, B. Nanostructured MnO₂: Hydrothermal synthesis and electrochemical properties as a supercapacitor electrode material. *J. Power Sources* **2006**, *159*, 361–364. [[CrossRef](#)]
35. Zhao, Y.; Meng, Y.; Jiang, P. Carbon@MnO₂ core-shell nanospheres for flexible high-performance supercapacitor electrode materials. *J. Power Sources* **2014**, *259*, 219–226. [[CrossRef](#)]
36. Du, M.; Wu, Y.; Hao, X. A facile chemical exfoliation method to obtain large size boron nitride nanosheets. *CrystEngComm* **2013**, *15*, 1782–1786. [[CrossRef](#)]
37. Wang, L.; Bai, Y.; Ma, Z.; Ge, C.; Guan, H.; Zhang, X. Tribological performances of hexagonal boron nitride nanosheets via surface modification with silane coupling agent. *SN Appl. Sci.* **2021**, *3*, 368. [[CrossRef](#)]
38. Mittal, N.; Kedawat, G.; Gupta, S.; Kumar Gupta, B. An Innovative Method for Large-Scale Synthesis of Hexagonal Boron Nitride Nanosheets by Liquid Phase Exfoliation. *ChemistrySelect* **2020**, *5*, 12564–12569. [[CrossRef](#)]
39. Azman, S.S.N.; Zulkifli, N.W.M.; Masjuki, H.; Gulzar, M.; Zahid, R. Study of tribological properties of lubricating oil blend added with graphene nanoplatelets. *J. Mater. Res.* **2016**, *31*, 1932–1938. [[CrossRef](#)]
40. Moshkovith, A.; Perfiliev, V.; Lapsker, I.; Fleischer, N.; Tenne, R.; Rapoport, L. Friction of fullerene-like WS₂ nanoparticles: Effect of agglomeration. *Tribol. Lett.* **2006**, *24*, 225–228. [[CrossRef](#)]
41. Rapoport, L.; Fleischer, N.; Tenne, R. Fullerene-like WS₂ Nanoparticles: Superior Lubricants for Harsh Conditions. *Adv. Mater.* **2003**, *15*, 651–655. [[CrossRef](#)]
42. Meng, Y.; Su, F.; Chen, Y. Supercritical Fluid Synthesis and Tribological Applications of Silver Nanoparticle-decorated Graphene in Engine Oil Nanofluid. *Sci. Rep.* **2016**, *6*, 31246. [[CrossRef](#)] [[PubMed](#)]
43. Fang, L.; Liu, D.M.; Guo, Y.; Liao, Z.M.; Luo, J.B.; Wen, S.Z. Thickness dependent friction on few-layer MoS₂, WS₂, and WSe₂. *Nanotechnology* **2017**, *28*, 245703. [[CrossRef](#)] [[PubMed](#)]
44. Lee, C.; Li, Q.; Kalb, W.; Liu, X.Z.; Berger, H.; Carpick, R.W.; Hone, J. Frictional characteristics of atomically thin sheets. *Science* **2010**, *328*, 76–80. [[CrossRef](#)]
45. Yamashita, T.; Hayes, P. Analysis of XPS spectra of Fe²⁺ and Fe³⁺ ions in oxide materials. *Appl. Surf. Sci.* **2008**, *254*, 2441–2449. [[CrossRef](#)]
46. Song, W.; Yan, J.; Ji, H. Fabrication of GNS/MoS₂ composite with different morphology and its tribological performance as a lubricant additive. *Appl. Surf. Sci.* **2019**, *469*, 226–235. [[CrossRef](#)]
47. Wu, X.; Gong, K.; Zhao, G.; Lou, W.; Wang, X.; Liu, W. MoS₂/WS₂ Quantum Dots as High-Performance Lubricant Additive in Polyalkylene Glycol for Steel/Steel Contact at Elevated Temperature. *Adv. Mater. Interfaces* **2017**, *5*, 1700859. [[CrossRef](#)]